Elastic scattering effects in the electron mean free path in a graphite overlayer studied by photoelectron spectroscopy and LEED

N. Barrett
CEA-DSM/DRECAM-SPCSI, CEA-Saclay, 91191 Gif-sur-Yvette, France

E. E. Krasovskii*
Institut für Theoretische Physik, Christian-Albrechts-Universität, D-24098 Kiel, Germany

J.-M. Themlin
L2MP, UMR CNRS 6137, Centre de Saint Jérôme, Université de Provence, Case 142, 13397 Marseille Cedex 20, France

V. N. Strocov
Swiss Light Source, Paul Scherrer Institute, CH-5232 Villigen PSI, Switzerland
(Received 2 October 2003; revised manuscript received 2 September 2004; published 31 January 2005)

The energy dependence of the mean free path $\lambda(E)$ in graphite at low kinetic energies (below ~50 eV) is studied using the synchrotron radiation excited Si 2*p* core level photoemission signal from a SiC substrate attenuated by an epitaxial graphite overlayer. Diffraction structure in $\lambda(E)$, appearing as strong intensity minima in the Si 2*p* signal, is found to reflect band gaps in the unoccupied states of graphite. Furthermore, $\lambda(E)$ is derived based on analysis of very-low-energy electron diffraction data supported by calculations of the complex band structure of unoccupied states, where $\lambda(E)$ appears from the Bloch wave damping factor. Conceptually different, the two methods yield equivalent $\lambda(E)$. The strength of the diffraction structure in $\lambda(E)$ manifests a significant elastic contribution to electron scattering at low energies, sharply increasing in the band gaps of the unoccupied states.

DOI: 10.1103/PhysRevB.71.035427 PACS number(s): 73.50.Bk, 79.60.−i, 71.20.Tx

I. INTRODUCTION

The electron mean free path λ plays a crucial role in surface sensitive electron spectroscopies,[1] such as photoemission spectroscopy, determining the relative strength of the surface and bulk contributions in the experimental spectra. Knowledge of the energy dependence of λ allows tuning of the electron kinetic energy to enhance or suppress the surface or bulk contributions, thus improving the reliability of the attribution of the different components.

λ is limited, first, by *inelastic* electron scattering due to the electron-electron and electron-phonon interactions. Its strength is expressed by a finite electron lifetime τ or, phenomenologically, by the imaginary part $V_i=\hbar/2\tau$ of the optical potential describing the electron absorption.[2,3] The inelastic scattering results in an energy dependence of λ, which is described by the well-known "universal curve" having a broad minimum around 50–100 eV.[1,4] This dependence is fairly similar for many materials. In addition, λ is limited by *elastic* electron scattering. This is due to diffraction off the crystal potential in certain energy and wave vector regions. From the band structure point of view, these are band gaps in the unoccupied states.[2,5,6] The elastic scattering results in *diffraction minima* of λ whose position and strength are critically material dependent. Such a diffraction structure of λ is particularly notable at very low energies, where the strength of the elastic and inelastic scattering can be comparable. It is particularly pronounced for layered materials with their highly modulated crystal potential.[5–7]

The most common method to measure λ is the *overlayer* method: an overlayer of the material under study is grown on top of a substrate, and attenuation of a substrate signal, usually a signal from a core level seen by photoelectron spectroscopy (PES), is measured.[1,4] Alternatively, λ can be determined from low-energy electron diffraction (LEED). The underlying assumption here is the logic of the one-step photoemission theory, which assumes that the surface sensitivity of the PES experiment comes from the decay of the time-reversed LEED wave function over a few atomic layers. In the LEED method λ appears in the damping factors of the Bloch wave constituents in the LEED wave function.[2,8] The quantitative LEED pattern is described by the diffracted electron current as a function of primary energy, $I(V)$, for each point. In fact, the maximum LEED spot intensities given by the $I(V)$ maxima mirror the diffraction minima of λ, whereas the broadening and the relative amplitudes of the $I(V)$ structures express the inelastic scattering. The LEED results are relevant for the photoemission experiment because the LEED state is related to the photoemission final state by time reversal.[9]

Here, we apply both methods to study the energy dependence of λ in graphite as a prototype layered material, focusing on the diffraction structures at very low energies (below ~50 eV). The overlayer method is applied to a single-crystal graphite film prepared by thermal epitaxial growth on SiC,[6,10] and employs PES measurements of the Si 2*p* core level signal. The LEED [or, in this energy range, very-low-energy electron diffraction (VLEED)] method in our implementation employs a different algorithm for accurate evaluation of V_i from broadening of the $I(V)$ spectral structures,

and full [non-muffin-tin (MT)] potential calculations of complex band structure[11] with the experimental V_i values. Some aspects of the theoretical analysis, arising from our *ab initio* evaluation of the LEED wave functions with V_i explicitly incorporated into the Hamiltonian, include determination of the transmitted current and attenuation length directly from the wave functions. This makes it possible to establish a relation between energy dependence of electron transmission and photocurrent attenuation, and offers insight into the phenomenon of inelastic scattering. We find the results of the overlayer and LEED methods in good agreement. Finally, details and methodology of the two methods are compared and discussed.

II. PHOTOEMISSION ATTENUATION IN OVERLAYER

A. Experimental procedure and results

The PES experiments were performed on the SA73 beamline of the SuperACO storage ring at LURE, France. All measurements were performed at normal emission. Linearly polarized monochromatic light from the plane grating monochromator was used with a polar incident angle of 45°.

The graphite/SiC overlayer system was prepared as described previously[6,10] by thermal epitaxial growth on the Si-terminated surface of 6*H*-SiC (0001). The substrate was cut from a commercial 0.3-mm-thick nitrogen-doped 6*H*-SiC wafer (CREE Research). It was fixed on a hollow Mo sample holder with an electron bombardment heating system on the underside. After introduction into the ultrahigh-vacuum chamber, the sample was heated to 850 °C under a Si flux from a resistively heated Si wafer. This cleaning procedure, which removes the native surface oxide, leads to a Si-rich 3×3 reconstruction as observed by LEED. The sample was then annealed for several minutes at temperatures above 1100 °C without the Si flux, which leads to the gradual development of a $(6\sqrt{3}\times6\sqrt{3})R30°$ LEED pattern. At these temperatures, SiC dissociates and Si sublimates, leaving C-rich surface layers that tend to form a graphite structure. These cycles were repeated several times, increasing the annealing temperature in the range [1250,1400] °C. The LEED spots characteristic of graphite become more and more intense, revealing a layer-by-layer growth of an epitaxial graphite film.

Crystallographic quality of the grown graphite film was confirmed by a sharp 1×1 LEED pattern without any visible rings indicative of azimuthal disorder. Its electronic structure was characterized by valence band PES measurements in a wide range of incident photon energies $h\nu$. With the normal emission geometry, they correspond to the layer-perpendicular ΓA direction of the bulk Brillouin zone of graphite. The results are presented in Fig. 1. We clearly observe well developed σ (close to 5 eV below E_F) and π (which disperses around 10 eV below E_F) states, characteristic of the bulk band structure. The spectra are indistinguishable from those of a bulk single crystal.[6,10,12,13] This confirms the identity of the overlayer electronic structure to that of bulk graphite, which is a prerequisite for legitimate comparison of the PES and VLEED results.

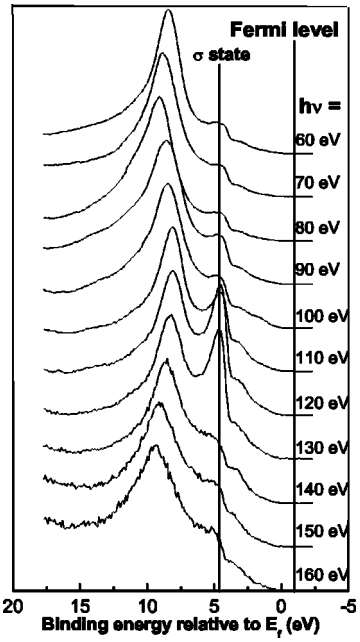

FIG. 1. Valence band spectra taken in a photon energy range of 60–160 eV. The σ and π states characteristic of crystalline graphite appear clearly.

The Si 2*p* core level emission (a binding energy of 99.2 eV in bulk Si and 101.5 eV in bulk SiC) spectra were measured as series of energy-distribution curves (EDCs) within a wide $h\nu$ range. The experimental EDCs are shown in Fig. 2. They have been normalized with respect to the incoming photon flux measured using the photocurrent I_0 emitted from a gold-plated grid at the entrance to the analysis chamber (another normalization using the level of the secondary electron background on the high kinetic energy side of the 2*p* emission yielded practically identical spectral intensities).

A comment to be made is the rather low Si 2*p* intensity. This is because we are measuring through a graphite overlayer whose thickness is much greater than λ. The satellites due to the SiC substrate surface reconstruction are no longer visible in LEED, implying that the overlayer thickness is at least three times λ of the low energy (around 100 eV) electrons. A reasonable estimate of the overlayer thickness from our previous characterizations[10,14] seems to be 20 Å. Thus the Si 2*p* signal is strongly attenuated. The empirical "universal" curve suggests an inelastic mean free path of between 5 and 10 Å at the kinetic energies measured. Based on the $\exp(-d/\lambda)$ relation, we would expect an attenuation of the Si underlayer signal of at least some 85% compared to that expected from clean SiC(0001). In order to improve the signal level, we limited the energy resolution to about 300 meV (obtained by convoluting the bandpass of the monochromator and the energy resolution of our hemispherical analyzer).

B. Si 2*p* line shapes

The Si 2*p* line shape characterizes chemical states of the Si atoms at the graphite/SiC interface. Through the whole experimental series the overall width of the Si 2*p* peak stays

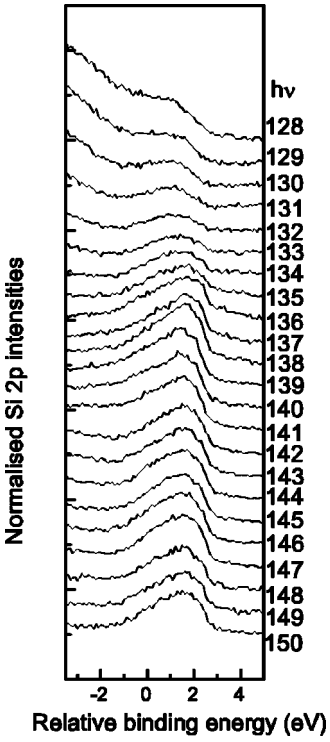

FIG. 2. Raw Si 2*p* spectra taken at normal emission angle for photon energies between 150 (lower spectrum) and 128 eV (upper spectrum) with steps of 1 eV. The energy scale is the binding energy determined with respect to the measured Fermi level.

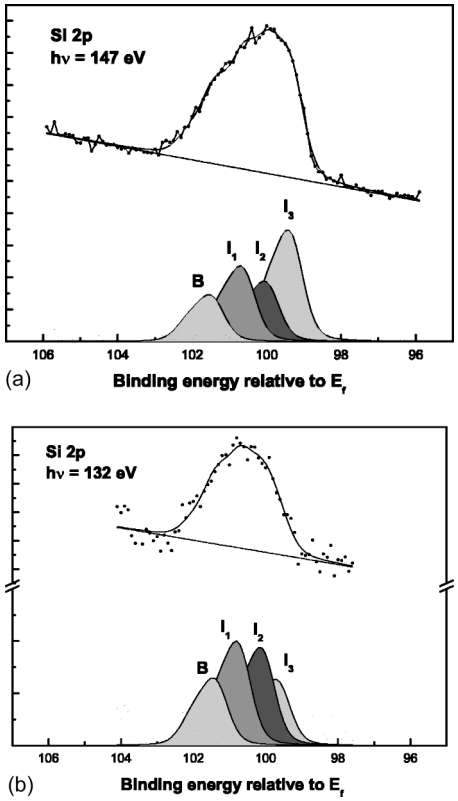

FIG. 3. Results of the core level analysis for two spectra (a) $h\upsilon = 147$ and (b) $h\upsilon = 132$ eV, corresponding to kinetic energies respectively outside and inside the final-state band gap for the 2*p* emission coming from the SiC substrate. The energy is given with respect to the Fermi level.

around 2.6–2.7 eV.[15] Given the natural 2*p* linewidth, there are obviously several components to the Si 2*p* line. To deconvolute them, we fitted the spectra using the RAINBOW program (©Spectral Software 1987–90, a program produced specifically for analyzing core level spectra). The fit parameters were chosen close to those normally used with the Si 2*p*: nearly linear background; spin-orbit splitting 0.6 eV; branching ratio 2; Doniach-Sunjic line shape with a Gaussian width of 0.7 eV (including the experimental resolution and the Si 2*p* spin-orbit splitting); Lorentzian width 0.2 eV; zero asymmetry. This latter assumption is justified by the low density of states at the Fermi level, seen in the valence band spectra in Fig. 1.

The best fits of the Si 2*p* spectra obtained for two different $h\upsilon$ values are presented in Fig. 3. The four components (because of the Gaussian width and poor statistics we do not distinguish the $2p_{3/2}$ from the $2p_{1/2}$) are labeled *B*, I_1, I_2, and I_3. Their energy positions are quite reproducible within the experimental statistics over all spectra obtained with 22 different photon energies. The most tightly bound peak *B* and the least tightly bound peak I_3 are found at 101.5 ± 0.38 eV and 99.24 ± 0.11 eV.[16] Following a recent study on thermal Si depletion of SiC,[15] the peak *B* corresponds to Si atoms in the regular tetrahedral environment of the bulk (unperturbed) SiC substrate under graphite. The other components I_1, I_2, and I_3 displaced toward the Fermi level, i.e., to weaker binding energies, are attributed to C-rich SiC under the graphite overlayer.

The existence of four Si 2*p* components implies that the interface between the graphite overlayer and the SiC substrate is not sharp, but embeds a continuous Si depth profile. This is not surprising given that the formation of the graphite layer is done via Si sublimation, and previous studies indeed suggest a depth profile.[14,15] The formation of graphite layers requires considerable Si mobility (for example, the complete Si depletion of three Si-C bilayers is necessary in order to form a single dense graphite layer). Johansson *et al.*[15] demonstrated the existence of multiple Si sites as a function of the SiC surface reconstruction and the near surface graphite content. For the $(6\sqrt{3} \times 6\sqrt{3})R30°$ reconstruction they also report four components, two of which are related to the bulk SiC, and the other two to the surface or subsurface regions. All of this is evidence that the final interface between the graphite overlayer and the SiC substrate, as perfect as the layer itself may be, largely extends into the bulk and drastically differs from the SiC structure itself. We have suggested the existence of a C-rich, essentially ordered diamondlike phase which is a precursor to graphite formation.[10] This precursor phase is characterized by C-C bonds with sp^3-hybridized C atoms, which is compatible with a particular C 1*s* component observed around 285.5 eV.[15] Apart from the small peak assigned to unperturbed "bulk" peak, the three components of the Si 2*p* which largely dominate the emission may thus be ascribed to specific defect or regular Si sites in this C-rich precursor, i.e., to Si bonded to fewer than four C neighbors.

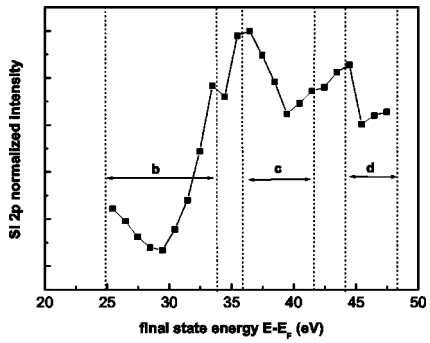

FIG. 4. The energy dependence of the Si 2*p* intensity, i.e., the area under the 2*p* peak, showing the attenuation in three energy regions, labeled *b*, *c*, and *d*: 25–34, 36–42, and 44–48 eV, which correlate in both energy position and width with the expected final-state band gaps indicated by dotted lines. The energy is given with respect to the Fermi level, allowing a direct comparison with the VLEED calculated final-state band structure.

C. Si 2*p* intensity energy dependence

In this paper we are mainly interested in the overall Si 2*p* core level intensity dependence on $h\nu$. From the Einstein equation for photoemission, the photoelectron kinetic energy is given by $E_{\mathrm{kin}}=h\nu-E_B-e\phi_{\mathrm{SP}}$. Here E_B is the binding energy and $e\phi_{\mathrm{SP}}$ the spectrometer work function (determined, as usual, from Fermi level measurements on the metal sample holder). The variation of $h\nu$ is equivalent to varying the kinetic energy of the photoelectron coming from the Si 2*p* core level after having traversed the graphite overlayer. The intensity variation of the Si 2*p* signal with $h\nu$ should therefore give a direct image of any strong elastic scattering due to band gaps of the unoccupied states through which the photoelectron transport takes place.

To extract the Si 2*p* intensity dependence, we have normalized each EDC to the continuous background level at 4 eV from the peak centroid position on the high-kinetic-energy side. This allows a direct comparison of the spectra, eliminating effects due to the synchrotron beam lifetime. We have also systematically measured the I_0 incoming photon flux using a gold grid at the entrance to the analysis chamber. The normalized intensities obtained by the two methods differed by less than 5%. The overall intensity of the Si 2*p* manifold (i.e., the integral area of the four Si 2*p* components after subtraction of the continuous linear background) as a function of the final-state energy of the Si 2*p* centroid with respect to the Fermi level is plotted in Fig. 4. In principle, our evaluation of the Si 2*p* intensity energy dependence from a series of EDCs is analogous to taking a constant initial-state (CIS) spectrum with the Si 2*p* initial state. We did not perform CIS measurements because of technical difficulties; however, via the core level shifts in the EDCs we have additionally obtained useful information on the chemical environment of Si atoms at the graphite/SiC interface.

To identify the origin of the observed Si 2*p* intensity variations, we have first analyzed the wave functions generated by our LEED calculations (see below). We have found that the character of the final-state wave function changes smoothly with energy, suggesting similar smooth variation of the tail of the wave function in the SiC substrate. Owing to the strong spatial localization of Si 2*p* states, the photoionization cross section is determined by the shape of the wave function (*s* and *d* orbitals) in the close vicinity of the nucleus. The energy interval over which these functions change considerably is of the order of 100 eV (the distance between two successive nodes at $r=1.8$ a.u.). Thus, we expect the variation of the atomic photoionization cross section to be of minor importance for the energy dependence of the Si 2*p* intensity. However, this point cannot be easily verified experimentally by PES measurements on uncovered SiC because, as noted above, the SiC surfaces reconstruct and are considerably different from the atomic arrangements at the graphite/SiC interface. Of the other factors determining the Si 2*p* intensity, the inelastic contribution to λ in the overlayer may be considered constant over a few eV. Thus, we attribute the observed structure in the Si 2*p* energy dependence to a strong elastic scattering in the final state due to band gaps. In particular, there are three strong attenuation regions of the Si 2*p* signal seen in Fig. 4, within 25–34 eV, 36–42 eV, and 44–48 eV. These regions line up well in both position and width with the band gaps found in the final states centered at 29, 39, and 46 eV relative to E_{F}, as indicated Fig. 4 (determination of the final-state band gaps from VLEED is presented below in Sec. III). Our data thus give direct evidence of diffraction structure of λ resulting from strong elastic scattering in the final-state band gaps.

An earlier study of the final-state energy dependence of the bulk core level emission in graphite clearly demonstrated the effect of the final-state band gaps at certain kinetic energies for the C 1*s* line.[7] Very recently a theoretical study of the effects of the overlayer electronic structure in photoelectron transmission has been reported.[17] However, to our knowledge our study gives the first experimental evidence of the effect of final states in photoemission coming from a substrate-overlayer system. Recent experiments on GaAs(100)-$c(4\times4)$ showed evidence for similar effects.[18] Such experiments allow a reliable distinction between the elastic and inelastic scattering contributions to λ.

III. VLEED

A. Nature of the final-state wave function

We recall that the relevance of LEED to the photoemission experiment is based on the fact that the LEED state is exactly the time-reversed photoemission final state.[9] A comment on the nature of the corresponding wave function $\Phi(\mathbf{r})$ should be made. In the mean free path analysis it is commonly implied that this wave function is described by one, single, exponentially decaying Bloch wave $\phi_k(\mathbf{r})$. The corresponding penetration depth λ is given by the imaginary part $\mathrm{Im}k_\perp$ of the surface-perpendicular wave vector as $(2\,\mathrm{Im}k_\perp)^{-1}$, where the factor 2 comes from the amplitude squaring for intensity. In fact, $\Phi(\mathbf{r})$ is a superposition $\Sigma_{\mathbf{k}}A_{\mathbf{k}}\phi_{\mathbf{k}}(\mathbf{r})$ of different Bloch wave constituents, each corresponding to different bands in $E(\mathbf{k})$. This can in principle complicate the mean free path analysis. (1) If a few $\phi_{\mathbf{k}}$ are comparable in amplitude, which is typical of highly hybrid-

ized band structures, the decay of the total $\Phi(\mathbf{r})$ becomes, strictly speaking, nonexponential and should be described by some effective λ depending on the individual penetration depths $\lambda_{\mathbf{k}}=(2\,\mathrm{Im}k_{\perp})^{-1}$ of the $\phi_{\mathbf{k}}(\mathbf{r})$ constituents as well as their relative $A_{\mathbf{k}}$ amplitudes. (2) In addition to the intrinsically bulk $\phi_{\mathbf{k}}$ with large $\lambda_{\mathbf{k}}$ (propagating in the $V_i=0$ limit) the total $\Phi(\mathbf{r})$ can contain intrinsically surface $\phi_{\mathbf{k}}$ with small $\lambda_{\mathbf{k}}$ (evanescent even in the $V_i=0$ limit). However, as the penetration depth of such surface $\phi_{\mathbf{k}}$ is much smaller than the interlayer distance, they are normally neglected in the electron transport picture.

B. Computational scheme

The theoretical LEED spectrum is derived from a self-consistent local density approximation density functional theory LDA-DFT based band structure calculation. The Kohn-Sham equations are solved with the extended linear augmented plane wave (ELAPW) $\mathbf{k}\cdot\mathbf{p}$ method.[19,20] The method of constructing the crystal potential and typical computational parameters are described elsewhere.[21] For graphite, our calculations have employed a basis set which included 585 energy-independent APWs (energy cutoff 28 Ry), and the extension of the radial basis set[20] contributed another 104 basis functions.

A detailed description of our *ab initio* method to calculate scattering wave functions (the LEED functions) within the complex band structure approach has already been presented.[11] Here we only briefly sketch the computational procedure.

We first solve the *inverse* complex-band-structure problem: given the crystal surface projection of the Bloch vector $\mathbf{k}_{//}$ and energy E, we find the complex $k_{\perp}$ values and the corresponding $\phi_{\mathbf{k}}(\mathbf{r})$ Bloch waves that satisfy the Schrödinger equation inside the crystal.[19] To circumvent the numerical instability of the matching formalism, we seek the total $\Phi(\mathbf{r})$ wave function as a linear combination of $\phi_{\mathbf{k}}(\mathbf{r})$ that continues smoothly into the vacuum half space, has a correct vacuum asymptotics, and minimizes the deviation $\|(\hat{\mathbf{H}}-E)\Phi\|$ from the exact solution everywhere in vacuum.[11] Such a variational matching procedure then leads to a system of linear equations on the $\phi_{\mathbf{k}}(\mathbf{r})$ amplitudes in the crystal and diffracted amplitudes in vacuum. The common choice of the matching plane at half the interlayer distance from the outermost atomic layer yielded in our case excellent agreement with the experiment (see below), and no further optimization of its position has been undertaken.

To describe the absorption due to inelastic scattering, we introduce the optical potential V_i into the Schrödinger equation as

$$\left[-\frac{\hbar^2}{2m}\Delta + V(\mathbf{r}) - iV_i - E\right]\phi(\mathbf{r}) = 0.$$

The larger the V_i value, the more smeared and reduced in amplitude the LEED spectral structures. The V_i was chosen to switch on at the matching plane. Its energy dependence $V_i(E)$ was extracted from the experimental normal-incidence VLEED spectrum[5] by varying the function $V_i(E)$ in the above equation so as to fit the calculated spectrum to the experiment.[11] New R factors were used to compare the experiment and calculations in terms of broadening and amplitude reduction of the spectral structures (see the Appendix). The experimental points were fitted to a superposition of an arctangentlike function and a polynomial function. The former models the increase of V_i through plasmon losses.[22]

In the absence of absorption the LEED wave function in the bulk half space far from the crystal surface is a superposition of propagating Bloch waves which carry current into the crystal interior. The absorption results in decay of the LEED function into the crystal interior, breaking down this picture. Nevertheless, the current at the crystal-vacuum interface is unambiguously determined by the asymptotic values of the incident and reflected currents in the vacuum, and can be interpreted as the transmitted current. To distinguish from the case of $V_i=0$, we refer to it as the *absorbed current*. It can be shown[3] that this current is determined by the electron density distribution in the decaying LEED state in the crystal, integrated from the matching plane to the bulk infinity:

$$T = \frac{2V_i}{\hbar}\int_{\Omega}|\Phi(\mathbf{r})|^2 d\mathbf{r}.$$

Here the integration is over the unit cell Ω of the semi-infinite crystal (infinite in the surface perpendicular direction) and T is the current through the base of Ω at the crystal-vacuum interface.[2] The accuracy of the calculations can be characterized by the residual mismatch of the transmitted current T calculated from the above formula with the total current calculated in the vacuum half space.

To characterize the electron transport properties of the individual Bloch waves, which are determined by both their $A_{\mathbf{k}}$ amplitude and $\lambda_{\mathbf{k}}$ penetration depth, we used *partial absorbed currents* $T_{\mathbf{k}}$ as the partial electron density integrated over the crystal interior via the formula

$$T_{\mathbf{k}} = \frac{2V_i}{\hbar}\int_{\Omega}|A_{\mathbf{k}}\phi_{\mathbf{k}}(\mathbf{r})|^2 d\mathbf{r}$$

which generalizes the $V_i=0$ elastic currents $-i|A_{\mathbf{k}}|^2(\hbar/2m)[\phi_{\mathbf{k}}^*(\partial/\partial r_{\perp})\phi_{\mathbf{k}}-\phi_{\mathbf{k}}(\partial/\partial r_{\perp})\phi_{\mathbf{k}}^*]$ for nonzero absorption.[3] Although in this case the $\phi_{\mathbf{k}}(\mathbf{r})$ interference in $\Phi(\mathbf{r})$ means that the total T is not exactly equal to the sum of the individual $T_{\mathbf{k}}$, these figures well characterize the relative contributions of the Bloch wave constituents to the total current transmitted by the LEED state.

By solving the LEED scattering problem with the experimental energy-dependent V_i we thus obtain the total $\Phi(\mathbf{r})$ wave function in the crystal expanded in the individual $\phi_{\mathbf{k}}(\mathbf{r})$ Bloch waves. This immediately gives our objective λ incorporating both inelastic and elastic scattering effects. An alternative LEED scheme to determine λ was recently advanced and applied to Cu.[8] The multiple scattering formalism with MT potential was used. The V_i energy dependence was taken from optical data. Significant anisotropic diffraction structure for Cu has been found in good agreement with the experiment. However, our scheme does have the advantages of (1) naturally taking into account the full-

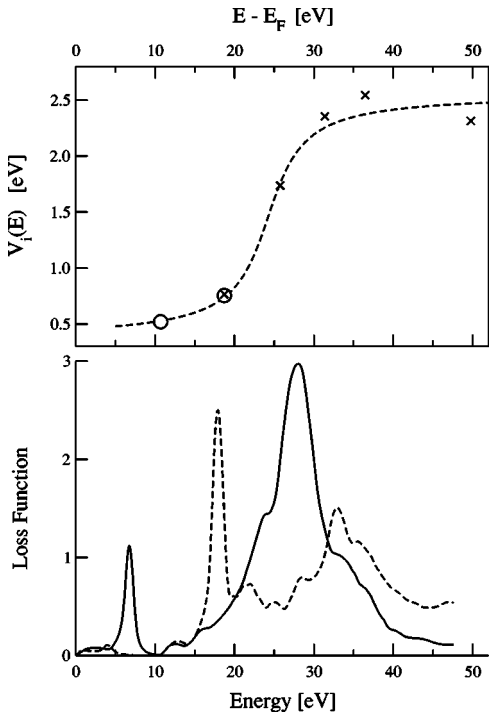

FIG. 5. Upper panel: Dependence of the optical potential $V_i(E)$ on the final-state energy determined from the sharpness of the $T(E)$ structures using the R_1 factor (circles) and from their normalized amplitude using the R_2 factor (crosses); see text. The dashed curve shows the analytical fit used in the LEED calculation. Lower panel: The loss function for $\mathbf{q}=\mathbf{0}$ for two directions of the $\mathbf{q}$ vector; $\mathbf{q}\perp\mathbf{c}$, full line, and $\mathbf{q}\|\mathbf{c}$, dashed line.

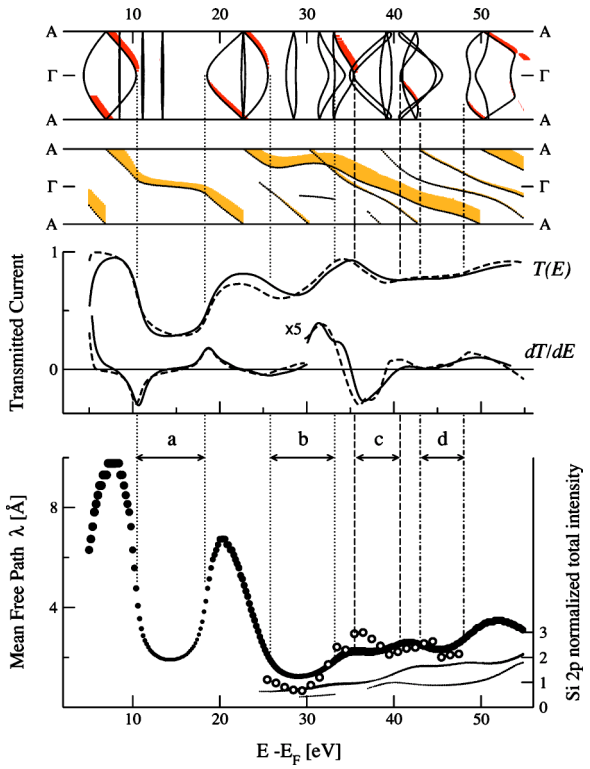

FIG. 6. (Color online) Top panel: Real and complex band structure $E(\mathrm{Re}k_\perp)$ of graphite in the ΓA direction, calculated with the experimental $V_i(E)$. The length of the tick parallel to the energy axis is proportional to the current carried by the Bloch constituent of the LEED function for $V_i=0$. In the lower graph of the upper panel is shown the complex band structure calculated with the experimental $V_i(E)$. The partial adsorbed currents $T_\mathbf{k}$ are shown as the thickness, i.e., perpendicular to the energy axis, of the curves. Middle panel: Electron transmission spectra $T(E)$ and dT/dE of graphite; experiment (full line) and theory (dashed line) calculated with the experimental $V_i(E)$. Bottom panel: Dependence of the attenuation length $\lambda_\mathbf{k}=(2\,\mathrm{Im}k_\perp)^{-1}$ of individual $\phi_\mathbf{k}$ on energy calculated with the experimental $V_i(E)$. The thickness of the curves is proportional to the associated $T_\mathbf{k}$. Shown are only $\phi_\mathbf{k}$ whose $T_\mathbf{k}$ exceeds 1% of the total current T as the total penetrating electron density. Open circles show the experimental Si 2*p* signal of Fig. 3 whose intensity scale is given on the right. The inset shows the region from 25 to 50 eV; it compares the theoretical curve shifted by 0.7 eV to higher energies with the energy dependence of the signal attenuation.

potential effects by employing the ELAPW method; and (2) being self-contained in that the V_i energy dependence is derived also from LEED. Note that in our scheme the Debye-Waller factor is already incorporated into V_i.

The next step in refining the above calculations would be to extend them to the real case of the whole graphite/SiC overlayer system. However, as can be deduced from Fig. 3, there are several interface sites for Si with very different neighborhoods, suggesting a complicated interface structure. Uncertainty about the geometry of such an interface has hindered calculations for the realistic graphite/SiC system.

C. Results

The experimental $V_i(E)$ energy dependence is presented in the upper panel of Fig. 5. It was derived from the experimental normal-incidence VLEED $T(E)$ spectrum[5] reproduced in the middle panel of Fig. 6 (despite the spectrum being measured in the target current mode, which reflects essentially the total electron reflectivity integrated over all diffracted beams, we use the term VLEED in reference to the dominant physical mechanism forming the spectral structures). The $V_i(E)$ dependence shows a sharp increase at around 25 eV.

In fact, the V_i optical potential is associated with the imaginary part of the electron self-energy Σ, whose energy dependence is expected to reflect singularities of the energy loss function $L(\omega)=-\mathrm{Im}[1/\varepsilon(\mathbf{q},\omega)]$. A rough idea of the average effect of plasmon excitations on the energy dependence of the electron lifetime can be obtained from the function $L(\omega)$ for $\mathbf{q}=\mathbf{0}$. In the lower panel of Fig. 5 we show our calculated loss function in the long wavelength limit for $\mathbf{q}\perp\mathbf{c}$ and $\mathbf{q}\|\mathbf{c}$, where $\mathbf{c}$ is the layer-perpendicular unit vector. Note the remarkably strong anisotropy of the loss function of graphite compared to transition metal dichalcogenides.[23] Our spectra agree well with the recent experimental and theoretical results[24] for $q=0.25$ Å^{-1}. It has been shown that by changing the orientation of the $\mathbf{q}$ vector from $\mathbf{q}\perp\mathbf{c}$ to $\mathbf{q}\|\mathbf{c}$ the high-energy bulk plasmon gradually moves from 28 to 18 eV and the loss function above 20 eV becomes more and more diffuse.[24] These results correlate well with the increase of V_i between 20 and 30 eV observed in our experimental $V_i(E)$ dependence.

The complex band structure calculated with the experimental $V_i(E)$ is shown in the top panel of Fig. 6 as $E(\mathrm{Re}k_\perp)$. Compared to the $V_i=0$ limit, also shown here, the effect of V_i is to smooth the band dispersions and smear the band gaps marked *a* to *d*. The $T_\mathbf{k}$ values, characterizing partial contributions of the individual damped Bloch waves to the *T* total current transmitted by the LEED state, are represented by the thickness of the curves. It is important to note that despite the multitude of bands only a few of them are effective in the electron transport.

The middle panel of Fig. 6 shows the theoretical $T(E)$ spectrum of graphite superimposed on the experimental one. Their dT/dE energy derivatives are also shown to emphasize the spectral structures. Excellent agreement of the theoretical and experimental results confirms our theoretical description of the LEED process. Systematic shifts of the experimental structures from their calculated positions by some 1 eV to higher energies manifest deviation of the quasiparticle self-energy Σ from the LDA-DFT exchange correlation, expressed by the $\Delta(\mathrm{Re}\Sigma)$ self-energy corrections.[5] The pronounced $T(E)$ minima, yielding a characteristic minimum-maximum structure in the dT/dE spectra, reveal the final-state band gaps *a* to *d*.[5]

Finally, the lower panel of Fig. 6 shows the $\lambda_\mathbf{k}=(2\,\mathrm{Im}k_\perp)^{-1}$ penetration depth of the individual $\varphi_\mathbf{k}(\mathbf{r})$ Bloch waves. Only the waves whose $T_\mathbf{k}$ partial currents exceed 1% of the total current into the crystal are shown. Thus, the evanescent $\varphi_\mathbf{k}(\mathbf{r})$ rapidly decaying into the crystal interior, and $\varphi_\mathbf{k}(\mathbf{r})$ with small excitation amplitudes $A_\mathbf{k}$, ineffective in the electron transport, are omitted. Below 25 eV only one $\varphi_\mathbf{k}(\mathbf{r})$ is seen. Its $\lambda_\mathbf{k}$ immediately gives our objective energy dependence $\lambda(E)$. Above 25 eV a few $\varphi_\mathbf{k}(\mathbf{r})$ with significant transport properties are seen. As discussed above, their existence in principle modifies the decay of the $\Phi(\mathbf{r})$ total wave field to a nonexponential one; however, in our case this effect is small because one $\varphi_\mathbf{k}(\mathbf{r})$ still much dominates in $T_\mathbf{k}$ and the corresponding $\lambda_\mathbf{k}$ is close to the overall λ.

The VLEED derived $\lambda(E)$ dependence shows pronounced diffraction minima in the final-state band gaps. Their energy position convincingly fits the three band gaps *b* to *d* observed in the experimental PES data from Fig. 4, reproduced here. The agreement of the VLEED and PES results improves even further if the $\Delta(\mathrm{Re}\Sigma)$ self-energy corrections, observed in the VLEED spectra, are applied to the $\lambda(E)$ curve. Qualitatively, the diffraction structure in $\lambda(E)$ is seen to mirror itself in the minima of the $T(E)$ spectrum due to the electron transmission reduction in the band gaps.

It should be noted that highly structured final states, as reflected in the VLEED spectra, are typical of the layered materials with essentially two-dimensional (2D) character due to sharp layer-perpendicular modulations of the crystal potential which open wide band gaps in the layer-perpendicular band dispersion.[11,25]

IV. DISCUSSION

A. Comparison of the PES- and VLEED-derived $\lambda(E)$ in graphite

The three observed broad diffraction minima in the PES signal are reproduced in the VLEED derived $\lambda(E)$ as to both energy positions and width, especially taking into account the self-energy corrections to the calculated curve. Note that the photoemission intensity depends upon $\exp(-d/\lambda)$, where *d* is the overlayer thickness, so only the energy positions may be compared directly. The agreement is convincing in view of the statistics of the PES measurements, and given the possible energy dependence of the photoexcitation matrix element and scattering at the substrate-overlayer interface (the effect of the latter on λ was discussed by McFeely *et al.*[26]). In particular, these effects should explain also the difference in the relative strength of the two $\lambda(E)$ minima in the PES and VLEED data. Unfortunately, due to drawbacks of our photoemission setup we could not extend the PES measurement to lower kinetic energies where the VLEED data show much stronger diffraction structure. All in all, we find the overlayer and VLEED methods give concurrent pictures of the $\lambda(E)$ behavior. The agreement achieved between the PES and VLEED results proves the relevance of our theoretical approach in which the graphite overlayer was replaced by bulk graphite.

B. Comparison of the overlayer and LEED methodology

The overlayer method has so far been the most common method to determine λ. Its advantages are physical clarity and straightforward data analysis. There are, however, serious limitations: (1) Preparation of a crystalline overlayer with sharp interface is experimentally difficult and not feasible for all materials; (2) variations in the photoexcitation matrix element can significantly influence the substrate signal; (3) determination of λ in absolute units from angle-dependent measurements can be hampered by $\mathbf{K}_{//}$-dependent diffraction effects.

The application of the VLEED method, fully taking into account the elastic and inelastic scattering, is done here, to our knowledge, for the first time. Its main advantage compared to the overlayer method is that it does not require any special sample preparations. Moreover, it involves one single-electron state and is therefore free of any matrix element effects. Certain limitations of this method include the following. (1) Significant computational effort. However, the computatonal procedure, if under well controlled numerical accuracy, is fully automatic in generating λ out of the experimental $V_i(E)$ and band calculations checked against the VLEED data. Moreover, the diffraction structure in $\lambda(E)$ can be assessed directly from the structure in $T(E)$ without any calculations. (2) The VLEED should be sufficiently rich in structures (which is the case for layered materials) to provide dense sampling of the V_i values in energy. Evaluation of $V_i(E)$ from off-normal VLEED spectra requires taking into account the absorption in the surface barrier which increases with $\mathbf{K}_{//}$.

Finally, it should be noted that there are, strictly speaking, certain differences between the final state as probed in the LEED and overlayer methods: whereas in the overlayer experiment the tail of the final-state wave function extends into the substrate, in the LEED experiment this wave function resides within the same material. However, in our case this difference is insignificant, as demonstrated by the valence

band spectra of the overlayer being identical to those of bulk graphite (see above Sec. II A).

C. Perspectives

The final-state effects (apart from the selection rules and when using polarized light) are not normally accounted for in the interpretation of photoemission data from localized states such as core levels. There is already growing awareness of the importance of the complex final-state band structure for accurate band structure studies.[6,27,28] However, our results demonstrate that final-state band gaps can strongly influence the photoemission intensity measured from underlayer core levels. This emphasizes the fact that the complex final-state band structure must be known in order to describe accurately the emission properties of crystalline solids.

Our results clearly have implications for the physics of the core level low-kinetic-energy photoelectron diffraction (PHD) from overlayer systems: This technique is often employed to determine the overlayer crystal structure from the substrate emission modulations in energy and $\mathbf{K}_{//}$ due to multiple scattering in the overlayer. This usually involves computationally expensive modeling of the multiple scattering within short-range approaches based on spherical waves and varying the crystal structure parameters. Equivalently, the multiple scattering can be viewed within a long-range picture, if the overlayer is thick enough, so as to create band gaps in the delocalized states in the overlayer for certain energy and $\mathbf{K}_{//}$ ranges. Such gaps are directly reflected in the $\mathbf{K}_{//}$ dispersion of the VLEED spectra of the overlayer. By combining VLEED and PHD, we could therefore predict the substrate core level emission modulations without any computational modeling. It would certainly be worthwhile carrying out a comparative VLEED and PHD study on a well defined overlayer model system to investigate such a connection between the two techniques.

V. CONCLUSION

Correlation of energy variations in the electron mean free path λ with band gaps in the photoelectron final state has been investigated for graphite as a prototype material with highly structured final states. The $\lambda(E)$ energy dependence was determined in an energy range below $\sim$50 eV using two conceptually different approaches, the overlayer method and VLEED. In the first approach, we used graphite overlayer grown on SiC and measured Si 2*p* core level PES signal from the substrate as a function of photoelectron kinetic energy. In the second approach, we used VLEED spectra measured on single-crystal graphite. Here, we have evaluated V_i, characterizing the strengths of inelastic scattering, from sharpness and relative amplitudes of the VLEED spectral structures, and then obtained λ as the damping factor of the LEED wave function in complex band structure calculations. The two approaches yielded essentially the same behavior of $\lambda(E)$, with some differences tracing back to the matrix element effects and influence of the overlayer/substrate interface in the overlayer method. Methodologically, the VLEED method benefits from the absence of such effects and the very need to have an overlayer system, but interpretation of the VLEED data is less straightforward and involves significant computational effort.

The experimental $\lambda(E)$ is characterized, in addition to the smooth "universal curve" energy dependence of the inelastic scattering, by pronounced diffraction structure reflecting variations in the elastic scattering off the crystal potential. The minima in $\lambda(E)$ manifest the final-state band gaps where the elastic scattering and the strength of photoelectron damping sharply increase. The diffraction structure in $\lambda(E)$ is particularly pronounced for graphite due to its essentially 2D character, resulting in wide band gaps. In perspective, the correlation between $\lambda(E)$ and final-state band gaps can find important implications not only in photoemission studies in the vuv range, but also in photoelectron diffraction studies where it affects the angular and energy-dependent anisotropies of the measured core level signal from both overlayer and single-crystal systems.

ACKNOWLEDGMENTS

We acknowledge the support of Deutsche Forschungsgemeinschaft to E.E.K. (Forschergruppe FOR 353) and to V.N.S. (CL124/5-1), and the EC support within the Access to Research Infrastructure program to V.N.S.

APPENDIX: EVALUATION OF V_i FROM VLEED SPECTRA

The inelastic scattering, expressed by the absorption potential V_i, manifests itself in the LEED spectra, whether it be those of individual diffracted beams $I(V)$, the integral electron reflection or the transmitted current $T(E)$, as a smearing of the spectral structures and a reduction in their amplitude. The values of V_i can therefore be extracted by comparison between theoretical spectra, calculated with different V_i, and experiment. However, *R* factors used in such a comparison must differ from the common *R* factors which tend to emphasize the energy position of the spectral peaks.

Following the ideas of our previous studies,[11,29] we develop here different *R* factors specialized in evaluation of V_i, particularly suitable for the VLEED energy range and for use with the $T(E)$ spectra. Such *R* factors should be designed along the following lines. (1) In the very-low-energy interval, the values of V_i are comparable with the widths of the band gaps, in which the elastic scattering gives rise to the reflectivity peaks. In this case the width of the spectral structures is largely due to the elastic reflection, while V_i manifests itself in the sharpness of the slopes of the spectral structures rather than in their width (see Fig. 6). Our *R* factors scrutinize therefore the *derived* dT/dE spectra emphasizing the slopes of the structures. (2) Energies of the spectral structures can be influenced by excited-state self-energy $\Delta\Sigma$ corrections with significant energy dependence beyond the DFT-based calculations. To make our *R* factors insensitive to the energy shifts, we do not use any integral comparison of the spectra, but determine values of the *R* factor *locally* at each dT/dE extremum. (3) The amplitudes of the dT/dE structures are partly influenced by the shape of the background in

$T(E)$ formed by inelastically reflected electrons, and by absorption in the surface barrier region which reduces the amplitudes of the spectral structures without their additional broadening. Ideally, a suitable R factor should be insensitive to the amplitudes.

We have found it convenient to use two such R factors. The first one is defined, for each dT/dE extremum, as $R_1 = (dT/dE)_{extr} / \int_{E_1}^{E_2} (dT/dE) dE$, where $(dT/dE)_{extr}$ is the extremal dT/dE value, and the integration is performed between the two dT/dE zeros with the energies E_1 and E_2 bounding the dT/dE extremum to yield the corresponding $T(E)$ excursion. While this R factor provides absolute values of V_i in each dT/dE extremum, it is sensitive to the overlap of the spectral structures and thus requires an energy separation much larger than V_i. In the case of graphite this condition was met only below 20 eV. For larger energies, we had to use another R factor, which relied on the reduction of the dT/dE extrema in amplitude *relative* to the lowest-energy one, as expressed by the ratio $R_2 = (dT/dE)_{extr} / (dT/dE)^0_{extr}$. Note that both R factors are independent of the constant background in $T(E)$. In addition, we suppressed their sensitivity to higher-order components by subtracting a quadratic background from both experimental and theoretical $T(E)$. To determine such a background, we identified the mid-slope points in the $T(E)$ structures as being placed at the extrema of dT/dE, and performed second-order polynomial fitting of the corresponding $T(E)$ values.

*Present address: Accelrys Inc., 334 Science Park, Cambridge CB4 0WN, UK.

[1] S. Hüfner, *Photoelectron Spectroscopy* (Springer, Berlin, 1996).
[2] J. B. Pendry, *Low Energy Electron Diffraction* (Academic Press, London, 1974).
[3] V. N. Strocov, H. Starnberg, and P. O. Nilsson, J. Phys.: Condens. Matter **8**, 7539 (1996); Phys. Rev. B **56**, 1717 (1997).
[4] D. R Penn, Phys. Rev. B **35**, 482 (1987).
[5] V. N. Strocov, P. Blaha, H. I. Starnberg, M. Rohlfing, R. Claessen, J.-M. Debever, and J.-M. Themlin, Phys. Rev. B **61**, 4994 (2000).
[6] V. N. Strocov, A. Charrier, J.-M. Themlin, M. Rohlfing, R. Claessen, N. Barrett, J. Avila, J. Sanchez, and M.-C. Asensio, Phys. Rev. B **64**, 075105 (2001).
[7] T. Balasubramanian, J. N. Andersen, and L. Walldén, Phys. Rev. B **64**, 205420 (2001).
[8] J. Rundgren, Phys. Rev. B **59**, 5106 (1999).
[9] P. J. Feibelman and D. E. Eastman, Phys. Rev. B **10**, 4932 (1974).
[10] I. Forbeaux, J.-M. Themlin, and J.-M. Debever, Phys. Rev. B **58**, 16 396 (1998).
[11] E. E. Krasovskii, W. Schattke, V. N. Strocov, and R. Claessen, Phys. Rev. B **66**, 235403 (2002).
[12] D. Marchand, C. Frétigny, M. Laguës, F. Batallan, Ch. Simon, I. Rosenman, and R. Pinchaux, Phys. Rev. B **30**, 4788 (1984).
[13] A. R. Law, M. T. Johnson, and H. P. Hughes, Phys. Rev. B **34**, 4289 (1986)
[14] A. Charrier, A. Coati, T. Argunova, F. Thibaudau, Y. Garreau, R. Pinchaux, I. Forbeaux, J.-M. Debever, M. Sauvage-Simkin, and J.-M. Themlin, J. Appl. Phys. **92**, 2479 (2002).
[15] L. I. Johansson, F. Owman, P. Mårtensson, Phys. Rev. B **53**, 13 793 (1996).
[16] The uncertainty is the standard deviation from the mean positions determined using a four-peak fit without imposing any constraints on the energy position obtained from the individual fits. It is greater for the bulk emission because its intensity is systematically weaker than that of the interface peaks.
[17] J. Henk, P. Bose, Th. Michael, and P. Bruno, Phys. Rev. B **68**, 052403 (2003).
[18] M. Cukr, P. Jiricek, J. Zemek, and I. Bartoš (unpublished).
[19] E. E. Krasovskii and W. Schattke, Phys. Rev. B **56**, 12 874 (1997).
[20] E. E. Krasovskii and W. Schattke, Phys. Rev. B **63**, 235112 (2001).
[21] E. E. Krasovskii, F. Starrost, and W. Schattke, Phys. Rev. B **59**, 10 504 (1999).
[22] T. Grandke, L. Ley, and M. Cardona, Phys. Rev. B **18**, 3847 (1978).
[23] W. Y. Liang, J. Phys. C **6**, 551 (1973).
[24] A. G. Marinopoulos, L. Reining, V. Olevano, A. Rubio, T. Pichler, X. Liu, M. Knupfer, and J. Fink, Phys. Rev. Lett. **89**, 076402 (2002).
[25] V. N. Strocov, *Electron Spectroscopies Applied to Low-Dimensional Materials* (Kluwer, Dordrecht, 2000).
[26] F. R. McFeely, E. Cartier, J. A. Yarmoff, and S. A. Joyce, Phys. Rev. B **42**, 5191 (1990).
[27] T. Strasser, C. Solterbeck, W. Schattke, I. Bartos, M. Cukr, P. Jiricek, C. S. Fadley, and M. A. Van Hove, Phys. Rev. B **63**, 195321 (2001).
[28] E. E. Krasovskii and W. Schattke, Phys. Rev. Lett. **93**, 027601 (2004).
[29] V. N. Strocov, H. I. Starnberg, P. O. Nilsson, H. E. Brauer, and L. J. Holleboom, J. Phys.: Condens. Matter **10**, 5749 (1998).